INRIA

INSTITUT NATIONAL DE RECHERCHE EN INFORMATIQUE ET EN AUTOMATIQUE

Fast in-flight detection of flutter onset - A statistical approach

Laurent Mevel, Michèle Basseville, Albert Benveniste

N°4982

Octobre 2003

THÈME 4

ISSN 0249-6399 ISRN INRIA/RR--4982--FR+ENG

Fast in-flight detection of flutter onset - A statistical approach

Laurent Mevel*, Michèle Basseville†, Albert Benveniste‡

Thème 4 — Simulation et optimisation
de systèmes complexes
Projet Sigma2

Rapport de recherche n ° 4982 — Octobre 2003 — 24 pages

Abstract: The flutter monitoring problem is investigated from a detection (and not prediction) point of view, and stated as a statistical hypotheses testing problem regarding a specified damping coefficient. Two flutter onset detection algorithms are described. Both tests build on a residual associated with an output-only subspace-based structural identification method, previously introduced by the authors for structural health monitoring. The first test, working batch wise, handles a null and a close alternative statistical hypotheses on the damping. It comes up from variations on a local asymptotic approximation for the residual, combined with the generalized likelihood ratio (GLR) test. The second test, working on-line, is based on non local hypotheses. It builds on a different approximation for the residual, combined with the cumulative sum (CUSUM) test of common use in quality control. Numerical results obtained on real data are discussed, which suggest some interesting properties of the on-line test.

Key-words: Subspace-based identification algorithms, change detection algorithms, statistical hypotheses testing, on-line detection, flutter monitoring, damping coefficient.

(Résumé : tsvp)

This work has been carried out within the framework of Eureka project no 2419 FLITE (**Fli**ght **T**est **E**asy), coordinated by Sopemea, Velizy-Villacoublay, France.

* IRISA/INRIA – Laurent.Mevel@irisa.fr.
† IRISA/CNRS – Michele.Basseville@irisa.fr.
‡ IRISA/INRIA – Albert.Benveniste@irisa.fr.

Unité de recherche INRIA Rennes
IRISA, Campus universitaire de Beaulieu, 35042 RENNES Cedex (France)
Téléphone : 02 99 84 71 00 - International : +33 2 99 84 71 00
Télécopie : 02 99 84 71 71 - International : +33 2 99 84 71 71

Détection embarquée du phénomène de flutter - Une approche statistique

Résumé : Le problème d'instabilité aérodynamique des avions, connu sous le nom de flutter, est abordé sous un angle de détection, et non pas de prédiction, et posé comme un problème de test d'hypothèses statistiques concernant un coefficient d'amortissement. On décrit deux algorithmes de détection de ce phénomène. Ces deux tests reposent sur le résidu associé à la méthode d'identification sous-espace que nous avons introduit dans le contexte de la surveillance d'intégrité de structures mécaniques. Le premier test, qui travaille sur des blocs de données, permet de choisir entre deux hypothèses proches. Il repose sur une variation de l'approximation asymptotique locale du résidu combinée à un test GLR. Le deuxième test, qui travaille en-ligne, permet de choisir entre deux hypothèses non locales. Il repose sur une autre approximation du résidu combinée au test (CUSUM) d'usage courant en contrôle de qualité. Des résultats numériques obtenus sur données réelles suggèrent des propriétés intéressantes du deuxième test.

Mots-clé : Algorithmes d'identification sous-espace, algorithmes de détection de changement, tests d'hypothèses statistiques, détection en-ligne, surveillance de flutter, coefficient d'amortissement.

1 Introduction

The development of new aircrafts requires a careful exploration of the dynamical behavior of the structure subject to vibration and aero-servo-elastic forces. This is achieved via a combination of ground vibration tests and in-flight tests. For both types of tests, various sensors data are recorded, and modal analyses are performed. Important challenges of the in-flight modal analyses are the limited choices for measured excitation inputs, and the presence of unmeasured natural excitation input (turbulence). A better exploitation of flight test data can be achieved by using output-only system identification methods, which exploits data recorded under natural excitation conditions (e.g., turbulent), without resorting to artificial control surface excitation and other types of excitation inputs [6, 24].

A crucial issue is to ensure that the newly designed airplane is stable throughout its operating range. A critical instability phenomenon, known under the name of *"aero-elastic flutter, involves the unfavorable interaction of aerodynamic, elastic, and inertia forces on structures to produce an unstable oscillation that often results in structural failure"* [17]. For preventing from this phenomenon, the airplane is submitted to a flight flutter testing procedure, with incrementally increasing altitude and airspeed. The problem of predicting the speed at which flutter can occur is usually addressed with the aid of identification methods achieving modal analysis from the in-flight data recorded during these tests [17, 8, 28, 20]. Three different levels are distinguished in [28]. The level 1 approach, basically handling one degree of freedom, counts zero crossings and computes log decrement damping on charts recording impulse decays, and captures only a single dominant mode. The level 2 approach uses multiple degrees of freedom methods for estimating global modal estimates (frequencies and damping coefficients), and is necessary when the mode of interest does not dominate the response. The level 3 approach estimates aerodynamic parameters and a stability boundary, for the purpose of flutter stability prediction [10, 31, 29]. The rationale of the first two approaches is that the damping coefficient reflects the rate of increase or decrease in energy in the aero-servo-elastic system, and thus is a relevant measure of stability. Therefore, while frequencies and modeshapes are usually the most important parameters in structural analysis, the most critical ones in flutter analysis are the damping factors, for some critical modes. The modeshapes are usually not estimated for flutter testing [28].

Until the late nineties, most approaches to flutter clearance have led to *data-based* methods, processing different types of data [20]. Many methods handle time-domain or frequency-domain functions, based on responses to impulse excitation or

atmospheric turbulence [37, 17, 14, 16, 33]. A comparison on data from the F-18 SRA, involving modern time and frequency domain subspace identification methods, is reported in [14]. Recent attempts at automating identification and classification of aero-elastic and aero-servo-elastic dynamics have been based on multiscale wavelet processing [9].

A *combined data-based and model-based* method has been introduced recently under the name of flutterometer [21, 22, 19]. Based on an aero-elastic state-space model and on frequency-domain transfer functions extracted from sensor data under controlled excitation, the flutterometer computes on-line a robust flutter margin using the μ-method for analyzing the worst case effects of model uncertainty. In recent comparative evaluations using simulated and real data [11, 20], several data-based methods are shown to fail in accurately predicting flutter when using data from low speed tests, whereas the flutterometer turns out not to converge to the true flutter speed during envelope expansion, due to inherent conservative predictions.

Algorithms achieving the *on-line in-flight* exploitation of flight test data are expected to allow a more direct exploration of the flight domain, with improved confidence and reduced costs. Among other challenges, one important issue to be addressed on-line is the flight flutter monitoring problem, stated as the problem of monitoring some specific damping coefficients. On the other hand, it is known, e.g. from Cramer-Rao bounds [15], that damping factors are difficult to estimate accurately. For improving the estimation of damping factors, and moreover for achieving this in real-time during flight tests, one possible although unexpected route is to resort to detection algorithms able to decide whether some damping factor decreases below some critical value or not. The rationale is that detection algorithms usually have a much shorter response time than identification algorithms.

The purpose of this paper is to describe and analyze two statistical tests for monitoring a damping factor. Both tests are based on a *residual* associated with a subspace-based output-only covariance-driven structural identification method. The residual is ideally zero under the hypothesis of constant modal parameters (null hypothesis), and significantly different from zero in the presence of a deviation in a specific damping coefficient (alternative hypothesis). The first test, called *local*, handles a null and an alternative statistical hypotheses on the damping which are close, and comes up from variations on a local asymptotic approximation for the residual, combined with the generalized likelihood ratio (GLR) test. The second test handles *non local* hypotheses, and builds on a different approximation for the residual combined with the cumulative sum (CUSUM) test.

The paper is organized as follows. Section 2 summarizes the main lines of the subspace-based monitoring residual investigated in earlier papers of the authors. In section 3, the first test for flutter monitoring, working batch wise and based on local hypotheses, is introduced. The second test, based on non local hypotheses, and performing on-line flutter monitoring, is described in section 4. Section 5 is devoted to implementation issues and experimental results obtained on real data. Some conclusions are drawn in section 6.

2 Subspace-based modal identification and monitoring

We first recall the main equations and parameters of the models we use, and we recall the main lines of the subspace-based covariance-driven identification and monitoring algorithms we advocate for.

2.1 Modeling and parameterizations

The structure's behavior is assumed to be described by a stationary linear system:

$$M\ddot{\mathcal{Z}}(t) + C\dot{\mathcal{Z}}(t) + K\mathcal{Z}(t) = \nu(t), Y(t) = L\mathcal{Z}(t) \tag{1}$$

where t denotes continuous time, M, C, K are the mass, damping and stiffness matrices respectively, (high dimensional) vector $\mathcal{Z}$ collects the displacements or accelerations of the degrees of freedom of the structure; the external (non measured) force ν is modeled as a non-stationary white noise with time-varying covariance matrix $Q_\nu(t)$, measurements are collected in the (often, low dimensional) vector Y, and matrix L indicates which components of the state vector are actually measured (where the sensors are located). The modes or eigen-frequencies denoted generically by μ, and the modeshapes or eigenvectors denoted generically by $L\Psi_\mu$, are solutions of:

$$\left\{ \begin{array}{rcl} \det\left(\mu^2\ M + \mu\ C + K\right) & = & 0 \\ \left(\mu^2\ M + \mu\ C + K\right)\ \Psi_\mu & = & 0 \end{array} \right. \tag{2}$$

Sampling model (1) at rate $1/\tau$ yields the discrete time model in state space form:

$$\left\{ \begin{array}{rcl} X_{k+1} & = & F\ X_k + V_{k+1} \\ Y_k & = & H\ X_k \end{array} \right. \tag{3}$$

where $X_k = \begin{pmatrix} \mathcal{Z}(k\tau) \\ \dot{\mathcal{Z}}(k\tau) \end{pmatrix}, Y_k = Y(k\tau), H = (L \;\; 0), F = e^{\mathcal{L}\tau}$, $\mathcal{L} = \begin{pmatrix} 0 & I \\ -M^{-1}K & -M^{-1}C \end{pmatrix}$, and state noise V_{k+1} is *unmeasured*, Gaussian, zero-mean, white, with covariance matrix:

$$Q_{k+1} \stackrel{\text{def}}{=} \mathbf{E}(V_{k+1}\, V_{k+1}^T) = \int_{k\tau}^{(k+1)\tau} e^{\mathcal{L}s}\, \widetilde{Q}(s)\, e^{\mathcal{L}^T s} ds,$$

where $\mathbf{E}(.)$ denotes the expectation operator and:

$$\widetilde{Q}(s) = \begin{pmatrix} 0 & 0 \\ 0 & M^{-1}Q_\nu(s)M^{-T} \end{pmatrix}$$

State X and observed output Y have dimensions $2m$ and r respectively, with r (often much) smaller than $2m$ in practice.

Let (λ, ϕ_λ) be the eigenstructure of the state transition matrix F, namely:

$$\det\,(F - \lambda\, I) = 0, \quad (F - \lambda\, I)\, \phi_\lambda = 0 \tag{4}$$

The modal parameters defined in (2) are equivalently found from the eigenstructure $(\lambda, \varphi_\lambda)$'s in (4) using:

$$e^{\tau\mu} = \lambda, \quad L\, \Psi_\mu = \phi_\lambda \stackrel{\text{def}}{=} H\, \varphi_\lambda$$

The frequency f and damping coefficient ρ are recovered from a given eigenvalue λ through:

$$f = a/2\pi\tau, \quad \rho = 100\, |b|/\sqrt{a^2 + b^2}, \quad \text{where} \quad a = |\arctan \Im(\lambda)/\Re(\lambda)|\,, \; b = \ln|\lambda| \tag{5}$$

Eigenvectors are real if proportional damping is assumed, that is $C = \alpha M + \beta K$. The λ's and ϕ_λ's are pairwise complex conjugate. We assume that the system has no multiple eigenvalues. In addition, 0 is *not* an eigenvalue of state transition matrix F. The collection of modes (λ, ϕ_λ) form a canonical parameterization – namely a parameterization invariant w.r.t. changes in the state basis – of the *pole part* of the system in (3), referred to as the system eigenstructure. Note that the system eigenstructure can equally be found from the AR part of a multivariable ARMA model equivalent to (3), but that the AR vector parameters are *not* canonical. From now on, the collection of modes is also considered as the system parameter θ:

$$\theta \stackrel{\text{def}}{=} \begin{pmatrix} \Lambda \\ \text{vec}\Phi \end{pmatrix} \tag{6}$$

In (6), Λ is the vector whose elements are the eigenvalues λ, Φ is the matrix whose columns are the ϕ_λ's, and vec is the column stacking operator. Parameter θ has size $(r+1)m$.

2.2 Residual associated with subspace identification

The key steps of the output-only covariance-driven subspace structural identification method are briefly recalled, and a characterization of the modal parameter in (6) is exhibited, from which the proposed residual is defined.

Let $R_i \stackrel{\text{def}}{=} \mathbf{E}\left(Y_k\ Y_{k-i}^T\right)$ and:

$$\mathcal{H}_{p+1,q} \stackrel{\text{def}}{=} \begin{pmatrix} R_0 & R_1 & \vdots & R_{q-1} \\ R_1 & R_2 & \vdots & R_q \\ \vdots & \vdots & \vdots & \vdots \\ R_p & R_{p+1} & \vdots & R_{p+q-1} \end{pmatrix} \stackrel{\text{def}}{=} \text{Hank}\,(R_i) \tag{7}$$

be the output covariance and Hankel matrices, respectively. Introducing the cross-covariance between the state and the observed outputs: $G \stackrel{\text{def}}{=} \mathbf{E}\left(X_k Y_k^T\right)$, direct computations of the R_i's from the equations (3) lead to: $R_i = HF^iG$, and to the well known [30] factorization:

$$\mathcal{H}_{p+1,q} = \mathcal{O}_{p+1}(H,F)\ \mathcal{C}_q(F,G) \tag{8}$$

where:

$$\mathcal{O}_{p+1}(H,F) \stackrel{\text{def}}{=} \begin{pmatrix} H \\ HF \\ \vdots \\ HF^p \end{pmatrix} \quad \text{and} \quad \mathcal{C}_q(F,G) \stackrel{\text{def}}{=} (G\ FG\ \cdots\ F^{q-1}G) \tag{9}$$

are the observability and controllability matrices, respectively. The observation matrix H is then found in the first block-row of the observability matrix $\mathcal{O}$. The state-transition matrix F is obtained from the shift invariance property of $\mathcal{O}$, namely:

$$\mathcal{O}_p^{\uparrow}(H,F) = \mathcal{O}_p(H,F)\ F, \qquad \text{where}\ \ \mathcal{O}_p^{\uparrow}(H,F) \stackrel{\text{def}}{=} \begin{pmatrix} HF \\ HF^2 \\ \vdots \\ HF^p \end{pmatrix}$$

Assuming $\mathrm{rank}(\mathcal{O}_p) = \dim F$, and thus that the number of block-rows in $\mathcal{H}_{p+1,q}$ is large enough, is mandatory for recovering F. The eigenstructure (λ, ϕ_λ) then results from (4).

Factorization (8) is the key for a characterization of the canonical parameter vector θ in (6), and for deriving the proposal residual. Choosing the eigenvectors of matrix F as a basis for the state space of model (3) yields the following *modal* representation of the observability matrix:

$$\mathcal{O}_{p+1}(\theta) = \begin{pmatrix} \Phi \\ \Phi\Delta \\ \vdots \\ \Phi\Delta^p \end{pmatrix} \tag{10}$$

where $\Delta \stackrel{\text{def}}{=} \mathrm{diag}(\Lambda)$, and Λ and Φ are as in (6). Whether a nominal parameter θ_0 is in agreement with a given output covariance sequence $(R_j)_j$ is characterized by [3, 34]:

$$\mathcal{O}_{p+1}(\theta_0) \text{ and } \mathcal{H}_{p+1,q} \text{ have the same left kernel space} \tag{11}$$

The left kernel space of matrix M is the kernel space of matrix M^T. The property (11) can be checked as follows. From the nominal θ_0, compute $\mathcal{O}_{p+1}(\theta_0)$ using (10), and perform e.g. a SVD of $\mathcal{O}_{p+1}(\theta_0)$ for extracting a matrix U such that:

$$U^T\, U = I_s \;\text{ and }\; U^T\, \mathcal{O}_{p+1}(\theta_0) = 0$$

Matrix U is not unique (two such matrices are related through a post-multiplication with an orthonormal matrix), but can be regarded as a function of θ_0. Then the characterization writes:

$$U(\theta_0)^T\, \mathcal{H}_{p+1,q} = 0 \tag{12}$$

Assume now that *a reference θ_0 and a new sample $Y_1, \ldots, Y_n$ are available.* For checking whether the data agree with θ_0, the idea is to compute the empirical Hankel matrix $\widehat{\mathcal{H}}_{p+1,q}$:

$$\widehat{\mathcal{H}}_{p+1,q} \stackrel{\text{def}}{=} \mathrm{Hank}\left(\widehat{R}_i\right), \quad \widehat{R}_i \stackrel{\text{def}}{=} 1/n \sum_{k=1}^{n} Y_k\, Y_{k-i}^T \tag{13}$$

and to define the residual vector:

$$\zeta_n(\theta_0) \stackrel{\text{def}}{=} \sqrt{n}\, \mathrm{vec}\left(U^T(\theta_0)\; \widehat{\mathcal{H}}_{p+1,q}\right) \tag{14}$$

Let θ be the actual parameter value for the system which generated the new data sample, and $\mathbf{E}_\theta$ be the expectation when the actual system parameter is θ. From (12), we know that:

$$\mathbf{E}_\theta\left(\zeta_n(\theta_0)\right) = 0 \quad \text{iff} \quad \theta = \theta_0$$

In other words, $\zeta_n(\theta_0)$ has zero mean when no change occurs in θ, and nonzero mean if a change occurs. Thus $\zeta_n(\theta_0)$ plays the role of a residual.

2.3 On-board χ^2-test for modal monitoring

Testing if $\theta = \theta_0$ holds true – or equivalently deciding that the residual ζ_n is *significantly* different from zero – requires the knowledge of the probability distribution of $\zeta_n(\theta_0)$. Unfortunately this distribution is generally unknown. One manner to circumvent this difficulty is to assume close hypotheses:

$$(\textit{Safe})\ \mathbf{H}_0 :\ \theta = \theta_0 \quad \text{and} \quad (\textit{Damaged})\ \mathbf{H}_1 :\ \theta = \theta_0 + \delta\theta/\sqrt{n} \tag{15}$$

where vector $\delta\theta$ is unknown, but fixed. Note that for large n, hypothesis $\mathbf{H}_1$ corresponds to *small* deviations in θ. This is the statistical local approach [36, 2, 1]. Define the mean deviation:

$$\mathcal{J}(\theta_0) \stackrel{\text{def}}{=} -\,1/\sqrt{n}\ \ \partial/\partial\theta\ \mathbf{E}_{\theta_0}\ \zeta_n(\theta)\ |_{\theta=\theta_0} \tag{16}$$

and the residual covariance matrix $\Sigma(\theta_0) \stackrel{\text{def}}{=} \lim_{n\to\infty}\ \mathbf{E}_{\theta_0}(\zeta_n\ \zeta_n^T)$. Then, provided that $\Sigma(\theta_0)$ is positive definite, and for all $\delta\theta$ (including $\delta\theta = 0$), the residual ζ_n in (14) is asymptotically Gaussian distributed [3] when assuming θ as in (15):

$$\zeta_n(\theta_0) \xrightarrow[n\to\infty]{} \mathcal{N}\left(\mathcal{J}(\theta_0)\ \delta\theta,\ \Sigma(\theta_0)\right) \tag{17}$$

where $\mathcal{N}(\mu, \Sigma)$ stands for the Gaussian (normal) distribution with mean vector μ and covariance matrix Σ. Thus a deviation $\delta\theta \neq 0$ in the system parameter θ is reflected into a change in the mean value of residual ζ_n. Note that matrices $\mathcal{J}(\theta_0)$ and $\Sigma(\theta_0)$ depend on neither n nor the deviation $\delta\theta$. They can be estimated prior to testing, using data on the safe system, just as the reference θ_0. Consistent estimates of $\mathcal{J}$, based on a data sample, are given in [3], and do *not* depend on the particular normalization of the eigenvectors φ_λ. The estimation of Σ is somewhat tricky [35, 36].

Let $\widehat{\mathcal{J}}$ and $\widehat{\Sigma}$ be consistent estimates of $\mathcal{J}(\theta_0)$ and $\Sigma(\theta_0)$, and assume that $\mathcal{J}(\theta_0)$ is f.c.r. Then, deciding whether residual ζ_n is *significantly* different from zero, stated

as testing the presence of a small deviation in θ (15), can be achieved with the aid of the generalized likelihood ratio (GLR) test based on the distribution (17), namely:

$$\begin{array}{l} + \sup_{\theta \in \mathbf{H}_1} \left(-(\zeta_n - \widehat{\mathcal{J}}\ \delta\theta)^T\ \widehat{\Sigma}^{-1} (\zeta_n - \widehat{\mathcal{J}}\ \delta\theta) \right) \\ - \sup_{\theta \in \mathbf{H}_0} \left(-(\zeta_n - \widehat{\mathcal{J}}\ \delta\theta)^T\ \widehat{\Sigma}^{-1} (\zeta_n - \widehat{\mathcal{J}}\ \delta\theta) \right) \\ = \sup_{\delta\theta \neq 0} \left(-(\zeta_n - \widehat{\mathcal{J}}\ \delta\theta)^T\ \widehat{\Sigma}^{-1} (\zeta_n - \widehat{\mathcal{J}}\ \delta\theta) \right) \ +\ \zeta_n\ \widehat{\Sigma}^{-1}\ \zeta_n \end{array} \tag{18}$$

This boils down to the following χ^2-test:

$$\chi^2_n(\theta_0) \stackrel{\text{def}}{=} \zeta_n^T(\theta_0)\ \widehat{\Sigma}^{-1}\ \widehat{\mathcal{J}} \left(\widehat{\mathcal{J}}^T\ \widehat{\Sigma}^{-1}\ \widehat{\mathcal{J}} \right)^{-1} \widehat{\mathcal{J}}^T\ \widehat{\Sigma}^{-1}\ \zeta_n(\theta_0) \tag{19}$$

which should be compared to a threshold. Note that the only term in (19) which is computed after data collection is $\zeta_n(\theta_0)$. Test $\chi^2_n(\theta_0)$ is asymptotically distributed as a χ^2-variable, with $\text{rank}(\mathcal{J})$ degrees of freedom and non-centrality parameter under $\mathbf{H}_1$: $\delta\theta^T \mathcal{J}^T \Sigma^{-1} \mathcal{J}\ \delta\theta$. In other words:

$$\begin{array}{rcl} \mathbf{E}_{\mathbf{H}_0}\ \chi^2_n(\theta_0) & = & \text{rank}(\mathcal{J}) \\ \mathbf{E}_{\mathbf{H}_1}\ \chi^2_n(\theta_0) & = & \text{rank}(\mathcal{J}) + \delta\theta^T\ \mathcal{J}^T\ \Sigma^{-1}\ \mathcal{J}\ \delta\theta \end{array} \tag{20}$$

In practice, however, the actual values of χ^2_n are much higher than those theoretical values. How to select a threshold for χ^2_n from histograms of empirical values obtained on data for undamaged cases is explained in [23].

2.4 Modal diagnosis

The modal diagnosis problem is to *decide which components* of θ have changed. Determining which eigenfrequencies and associated modeshapes have been affected by the damage is often addressed as an estimation problem, based on modal identification in the pre- and post-damage stages [13]. We address modal diagnosis as a *detection* problem instead, using the estimated Jacobian matrix $\widehat{\mathcal{J}}_i$ corresponding to mode and modeshape i [4]. The directional test focussed on this mode i writes:

$$\chi^{(i)2}_n \stackrel{\text{def}}{=} \zeta_n^T\ \widehat{\Sigma}^{-1}\ \widehat{\mathcal{J}}_i\ \left(\widehat{\mathcal{J}}_i^T\ \widehat{\Sigma}^{-1}\ \widehat{\mathcal{J}}_i \right)^{-1}\ \widehat{\mathcal{J}}_i^T\ \widehat{\Sigma}^{-1}\ \zeta_n \tag{21}$$

Such a directional test restricted to the damping coefficient ρ of a given mode defined in (5) could be designed as a solution to the flutter monitoring problem. However, the relevant hypotheses for that problem should be one-sided, which is not the case in (15). This calls for a further step in the design of flutter monitoring tests, as described next. In what follows, the $\widehat{\ }$ above $\mathcal{J}$ and Σ are dropped for simplicity.

3 Flutter monitoring - First test, working batch wise

As explained in the introduction, one manner to address the flutter problem is basically to decide whether some damping coefficient ρ decreases below some specified critical value ρ_c, namely:

$$\rho < \rho_c \tag{22}$$

In this section, we describe a first test for solving this problem. This test handles a null and a close alternative hypotheses on the damping coefficient, and comes up from variations on the statistical local approach for the residual, combined with the GLR test (18).

In this paper, we assume that $\rho_c = \rho_0$, where ρ_0 is the actual value of the monitored damping coefficient, in the reference parameter θ_0. The realistic case $\rho_c < \rho_0$ is the topic of current investigations and will be reported elsewhere. See the discussion at the end of paper.

As before, the observed data is considered to consist of the residual defined in (14):

$$\zeta \stackrel{\text{def}}{=} \zeta(\theta_0)$$

Let $\mathcal{J} \stackrel{\text{def}}{=} \mathcal{J}(\rho_0)$ be the Jacobian matrix corresponding to the damping coefficient ρ_0, and $\Sigma \stackrel{\text{def}}{=} \Sigma(\theta_0)$ be the residual covariance matrix. The matrix $\mathcal{J} \stackrel{\text{def}}{=} \mathcal{J}(\rho_0)$ is obtained by selecting the corresponding column of the matrix which results from the multiplication of $\mathcal{J}(\theta_0)$ with the Jacobian of the transformation (5) from the $\lambda' s$ to the $\rho' s$ [4] Reminding (19), we introduce:

$$\overline{\zeta} \stackrel{\text{def}}{=} \mathcal{J}^T \, \Sigma^{-1} \, \zeta, \quad \overline{\Sigma} \stackrel{\text{def}}{=} \mathcal{J}^T \, \Sigma^{-1} \, \mathcal{J} \tag{23}$$

Note that these are scalar numbers. It results from (17) that, when assuming $\rho = \rho_0 + \delta\rho/\sqrt{n}$, for all $\delta\rho$, the residual ζ_n in (14) is asymptotically Gaussian:

$$\overline{\zeta} \xrightarrow[n \to \infty]{} \mathcal{N}(\overline{\Sigma} \, \delta\rho, \overline{\Sigma}) \tag{24}$$

3.1 A one-sided test

Consider the following *local* hypotheses:

$$\mathbf{H}_0 : \ \delta\rho \geq 0 \quad \text{and} \quad \mathbf{H}_1 : \ \delta\rho < 0 \tag{25}$$

which express that the damping coefficient decreases below ρ_0 while remaining in close neighborhoods. The GLR test for the testing problem (25), namely:

$$l(\theta_0) \stackrel{\text{def}}{=} \sup_{\delta\rho<0} \left(-(\overline{\zeta} - \overline{\Sigma}\,\delta\rho)^T\,\overline{\Sigma}^{-1}\,(\overline{\zeta} - \overline{\Sigma}\,\delta\rho)\right) - \sup_{\delta\rho\geq 0} \left(-(\overline{\zeta} - \overline{\Sigma}\,\delta\rho)^T\,\overline{\Sigma}^{-1}\,(\overline{\zeta} - \overline{\Sigma}\,\delta\rho)\right) \tag{26}$$

can be shown [18] to boil down to:

$$l(\theta_0) \;=\; -\;\text{sign}(\overline{\zeta})\cdot\overline{\chi}^2, \quad \overline{\chi}^2 \stackrel{\text{def}}{=} \overline{\zeta}^T\,\overline{\Sigma}^{-1}\,\overline{\zeta} \tag{27}$$

The test statistics $l(\theta_0)$ enjoys the following property:

$$\mathbf{E}_{\mathbf{H}_0}\; l(\theta_0) \;\leq\; 0 \tag{28}$$

$$\mathbf{E}_{\mathbf{H}_1}\; l(\theta_0) \;>\; 0 \tag{29}$$

In other words, it manifests itself the change in $\delta\rho$ by a change in its own sign. Thus it is a good candidate for solving the hypotheses testing problem in (25).

To sum up, the first test statistics proposed for flutter monitoring is defined by:

$$\zeta_n(\widetilde{\theta}_0) \;=\; \sqrt{n}\;\text{vec}\left(U^T(\theta_0)\;\widehat{\mathcal{H}}_{p+1,q}\right) \tag{30}$$

$$\begin{aligned} \overline{\zeta} \;&=\; \mathcal{J}^T\,\Sigma^{-1}\,\zeta_n, \quad \overline{\Sigma} \;=\; \mathcal{J}^T\,\Sigma^{-1}\,\mathcal{J} \\ \overline{\chi}^2 \;&=\; \overline{\zeta}^T\,\overline{\Sigma}^{-1}\,\overline{\zeta} \\ l(\theta_0) \;&=\; -\;\text{sign}(\overline{\zeta})\cdot\overline{\chi}^2 \end{aligned} \tag{31}$$

and a decision in favor of $\mathbf{H}_1$ is made when:

$$l(\theta_0) \geq \lambda \tag{32}$$

for some positive threshold λ to be chosen.

4 Flutter monitoring - Second test, working on-line

In this section, another decision function is introduced, as a first attempt to design an *on-line* flutter monitoring algorithm. This test builds on a different computation for the *same* residual $\zeta_n(\theta_0)$, no longer covariance-driven but now temporal data-driven. It also builds on a different approximation for $\zeta_n(\theta_0)$, and on the CUSUM test statistics [2].

4.1 Another insight in the residual

Because of (13), formula (30) for $\zeta_n(\theta_0)$ rewrites as:

$$\zeta_n(\theta_0) \;=\; \sum_{k=1}^{n} Z_k(\theta_0) \;/\sqrt{n} \tag{33}$$

where:

$$Z_k(\theta_0) \;\stackrel{\text{def}}{=}\; \text{vec}\left(U^T(\theta_0)\; \mathcal{Y}^+_{k,p+1}\; {\mathcal{Y}^-_{k,q}}^T\right) \tag{34}$$

and

$$\mathcal{Y}^+_{k,p+1} \stackrel{\text{def}}{=} \begin{pmatrix} Y_k \\ \vdots \\ Y_{k+p} \end{pmatrix}, \quad \mathcal{Y}^-_{k,q} \stackrel{\text{def}}{=} \begin{pmatrix} Y_k \\ \vdots \\ Y_{k-q+1} \end{pmatrix} \tag{35}$$

From (17), we know that $\zeta_n(\theta_0)$, and thus $\sum_{k=1}^n Z_k(\theta_0)/\sqrt{n}$, is asymptotically Gaussian distributed, with zero mean under the hypothesis $\rho = \rho_c$. Following the arguments in [7][5.4.1], it is legitimate to deduce from this fact the following approximation: for k large enough, $Z_k(\theta_0)$ is asymptotically Gaussian distributed, with *zero mean* under $\rho = \rho_c$, and the Z_k's are *independent*. Furthermore, a change from $\rho > \rho_c$ to $\rho < \rho_c$ is reflected by a change in the mean of $Z_k(\theta_0)$.

4.2 The CUSUM test

Consider now the following *non local* hypotheses:

$$\tilde{\mathbf{H}}_0 :\; \rho = \rho_c + \epsilon \quad \text{and} \quad \tilde{\mathbf{H}}_1 :\; \rho = \rho_c - \epsilon \tag{36}$$

with $\epsilon > 0$. Because the Z_k's can be considered as independent Gaussian variables, which manifest themselves a decrease in the damping by a change in their own mean value, testing between the hypotheses (36) can be addressed with the aid of the CUSUM test of common use in quality control. The CUSUM test statistics g_n is defined as follows [2]:

$$S_n(\theta_0) \;\stackrel{\text{def}}{=}\; \sum_{k=1}^{n} Z_k(\theta_0) \tag{37}$$

$$T_n(\theta_0) \;\stackrel{\text{def}}{=}\; \max_{1\le k\le n} S_k(\theta_0)$$

$$g_n(\theta_0) \;\stackrel{\text{def}}{=}\; T_n(\theta_0) - S_n(\theta_0) \tag{38}$$

A decision in favor of $\widetilde{\mathbf{H}}_1$ is made when:

$$g_n(\theta_0) \geq \lambda \tag{39}$$

for some threshold λ to be chosen.

Note that g_n monitors *on-line* the deviations of the cumulative sum S_n w.r.t. its maximum value T_n. In other words, the sum S_n is confronted to an *adaptive threshold*: $S_n \leq T_n - \lambda$.

Now, from (33), (37) and (34), we have:

$$S_n(\theta_0) = \sqrt{n}\ \zeta_n(\theta_0) = \sum_{k=1}^{n} \mathrm{vec}\left(U^T(\theta_0)\ \mathcal{Y}^+_{k,p+1}\ \mathcal{Y}^{-\ T}_{k,q}\right) \tag{40}$$

From (40), we deduce that test g_n in (38) handles the *time-unnormalized* residual $\zeta_n(\theta_0)$.

For numerical efficiency, it is preferable to normalize $S_n(\theta_0)$ in order to handle identity covariance matrices for all parameter values θ_0; remember (24). This is achieved by using the *scale-normalized* residual $\overline{\zeta}_n(\theta_0)$ as in (23), and computing, instead of (40) and (38):

$$\begin{aligned}
\overline{S}_n(\theta_0) &\stackrel{\text{def}}{=} \sqrt{n}\ \ \overline{\Sigma}(\theta_0)^{-1/2}\ \ \overline{\zeta}_n(\theta_0) \\
\overline{T}_n(\theta_0) &\stackrel{\text{def}}{=} \max_{1\leq k\leq n} \overline{S}_k(\theta_0) \\
\overline{g}_n(\theta_0) &\stackrel{\text{def}}{=} \overline{T}_n(\theta_0) - \overline{S}_n(\theta_0)
\end{aligned} \tag{41}$$

From its design, test statistics $\overline{g}_n(\theta_0)$ enjoys the following properties:

$$\begin{aligned}
\mathbf{E}_{\widetilde{\mathbf{H}}_0}\ \overline{g}_n(\theta_0) &\approx 0 \\
\mathbf{E}_{\widetilde{\mathbf{H}}_1}\ \overline{g}_n(\theta_0) &> 0
\end{aligned} \tag{42}$$

Moreover, if ρ decreases, $\overline{g}_n(\theta_0)$ increases.

4.3 The proposed on-line flutter test

Since it is known neither what is the actual hypothesis when this processing starts, nor what are the actual sign and magnitude of the change in ρ that will occur, a relevant procedure [2] consists in:

- Introducing a *minimum magnitude of change* ν_m;

- Running two tests in parallel, for decreasing and increasing damping, respectively;
- Making a decision according to the first test which fires;
- Switching to the other one afterwards.

At a first glance, having to tune an additional parameter may appear as a drawback. It turns out, however, that the choices of the minimum magnitude of change ν_m and of the threshold λ are generally well decoupled [2]. This algorithm is summarized in the following formulas, where the dependency in θ_0 is dropped for simplicity.
Decreasing damping:

$$\overline{S}_n^{(-)} \stackrel{\text{def}}{=} \overline{\Sigma}^{-1/2} \sum_{k=1}^{n} \left(\mathcal{J}^T \ \Sigma^{-1} \ Z_k + \nu_m \right) \tag{43}$$

$$\overline{T}_n \stackrel{\text{def}}{=} \max_{1 \le k \le n} \overline{S}_k^{(-)} \tag{44}$$

$$g_n^- \stackrel{\text{def}}{=} \overline{T}_n - \overline{S}_n^{(-)} \tag{45}$$

$$g_n^- \geq \lambda^- \tag{46}$$

Increasing damping:

$$\overline{S}_n^{(+)} \stackrel{\text{def}}{=} \overline{\Sigma}^{-1/2} \sum_{k=1}^{n} \left(\mathcal{J}^T \ \Sigma^{-1} \ Z_k - \nu_m \right) \tag{47}$$

$$\overline{t}_n \stackrel{\text{def}}{=} \min_{1 \le k \le n} \overline{S}_k^{(+)} \tag{48}$$

$$g_n^+ \stackrel{\text{def}}{=} \overline{S}_n^{(+)} - \overline{t}_n \tag{49}$$

$$g_n^+ \geq \lambda^+ \tag{50}$$

When (46) happens, both cumulative sums $\overline{S}_n^{(-)}$ and $\overline{S}_n^{(+)}$, and both extrema $\overline{T}_n$ and $\overline{t}_n$, are reset to zero, and g_n^+ is activated. As soon as (50) happens, both cumulative sums $\overline{S}_n^{(-)}$ and $\overline{S}_n^{(+)}$ and both extrema are reset to zero, and g_n^- is activated. This processing is made clear on the subsequent figures in the following manner. Let $t_i, i = 1, \ldots$ be the alarm *and* switch time instants. The actual test statistics f_t corresponding to the processing described above is defined by:

$$\forall t \in [t_k, t_{k+1}] \quad f_t \stackrel{\text{def}}{=} \begin{cases} -\ g_t^+ & \text{if } f_t = g_t^- > 0 \quad \forall t \in [t_{k-1}, t_k] \\ \quad g_t^- & \text{if } f_t = g_t^+ > 0 \quad \forall t \in [t_{k-1}, t_k] \end{cases} \tag{51}$$

This is the test statistics which is plotted on Figs. 2 and 3.

Since the test statistics g_n^- is devoted to the detection of a drop in the damping, $f_t = -\,g_t^-$ is plotted in red, in order to better visualize a drop. Similarly, since the test statistics g_n^+ is devoted to the detection of an increase in the damping, $f_t = g_t^+$ is plotted in blue. We stress that $\|f_t\|$ is small when $\rho >> \rho_c$, and large when ρ is close to, or crosses, ρ_c. When inspecting Figs. 2 and 3, it is important to keep in mind this intuitively desirable and very useful property.

5 Experimental analysis

The tests statistics $l(\theta_0)$ (31) and $\overline{g}_n(\theta_0)$ (41) are currently experimented on different data sets available within the Eureka project FLITE[1], aiming at improving the exploitation of flight test data, for enabling more direct exploration of the flight domain, with improved confidence and at reduced cost. In this paper, we discuss results obtained on a nonstationary data set recorded on a *real* flight structure, provided by one of the industrial partners. For obvious reasons, the actual values of the damping coefficient and the frequency are not displayed.

5.1 Implementation and tuning issues

Automatic modal analysis and flutter monitoring (monitoring one damping coefficient) have been performed using the Scilab Modal Analysis and damage detection and localization toolbox [26].

It should be stressed that the proposed flutter monitoring algorithm (51) can be computed in real time, whereas automatic modal identification is both computationally expensive and subject to estimation errors especially in the damping factors. Actually, the proposed damping test does *not* require re-identification of the damping coefficient at every step. Thus, it is much faster, and free from estimation error propagation.

For tuning the proposed algorithm, the user has to choose a minimum magnitude of change ν_m and a threshold λ. This should be done by extensive manual training – which has not been possible in the present example, due to lack of reference data – and can be achieved based on the following remarks.

- The threshold λ should be high enough to avoid reactions to small fluctuations, and small enough to allow quick detection. A small λ will lead to a constantly

[1] http://www.irisa.fr/sigma2/flite/

switching flutter test. On the contrary, a high λ would yield missed detection of changes in the evolution of the damping.

- The minimum magnitude of change ν_m should be chosen close to zero. A zero value lead to a flutter test with high fluctuations around the critical damping value. Increasing the value of ν_m would smooth out the test and remove false alarms. If ν_m gets too high, this kills the test, which no longer reacts at all.

5.2 Experimental results

The results of the automatic modal analysis for the considered mode (frequency and damping coefficient) are displayed on Fig. 1. It appears clearly that, whereas the frequency is slowly increasing, the damping coefficient exhibit large fluctuations. Notice that the change in the frequency is linear except in two places, where unexpected jumps happen in the estimation, which implies overestimation of the corresponding damping values (see the narrow peaks in the plot).

The first test statistics $l(\theta_0)$ (31) has shown up a very poor behavior, and thus is not displayed.

On Figs. 2 and 3, respectively, the behavior of the test statistics f_t in (51) is displayed for two different values of the critical damping: $\rho_c = \rho_0 = \rho_c^{(1)}$ and $\rho_c = \rho_0 = \rho_c^{(2)}$, with $\rho_c^{(2)} < \rho_c^{(1)}$. It should be noted that the time axis has not exactly the same meaning for Fig. 1 on the one hand, and Figs. 2 and 3 on the other hand. This is because of long batch processing for the former, and smaller batch and on-line processing, respectively, for the two latter. The intuitively obvious lower quality of the results in the early left portion of each figure should also be kept in mind.

Nevertheless, it clearly appears that the time intervals during which alarms are fired (the red statistics crossing its threshold) mainly correspond to the time periods with low damping values. Note also the coherent behavior of the tests on Figs. 2 and 3: if the test declares that the damping value is below $\rho_c^{(2)}$, it also declares that the damping value is below $\rho_c^{(1)}$.

5.3 Discussion

When monitoring multiple damping coefficients, different values for the threshold λ and magnitude ν_m could be used. Different values of ν_m for each of the two CUSUM tests g_n^- and g_n^+ could also be used for multiple testing. The rationale is as follows. A small change magnitude ν_m for test g_n^+ is likely to be relevant for an instantaneous

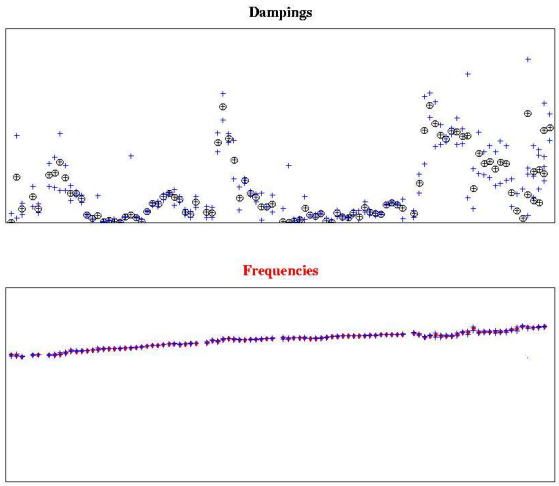

Figure 1: Automatic identification of one frequency (bottom) and damping coefficient (top).

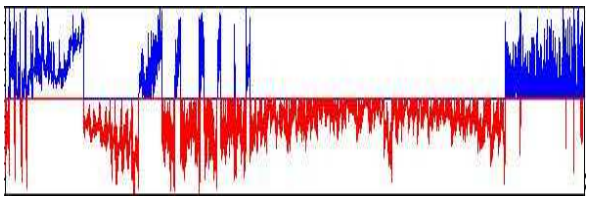

Figure 2: Test f_t for $\rho_c = \rho_c^{(1)}$. Bottom (red): $-g_n^-$ reflects $\rho < \rho_c$. Top (blue): g_n^+ reflects $\rho > \rho_c$.

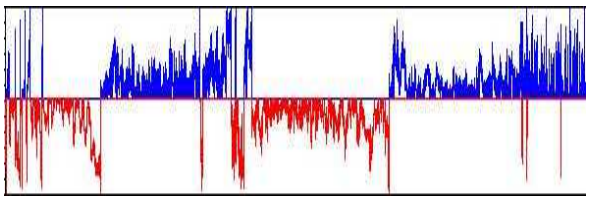

Figure 3: Test f_t for $\rho_c = \rho_c^{(2)} < \rho_c^{(1)}$. Bottom (red): $-g_n^-$ reflects $\rho < \rho_c$. Top (blue): g_n^+ reflects $\rho > \rho_c$.

reaction when ρ crosses the damping value ρ_c from above and towards zero. On the contrary, a larger ν_m should be used for making sure that the decision in favor of the safe hypothesis $\rho > \rho_c$ is correct with high probability.

This type of tuning could also be used for handling the more realistic case $\rho_c \neq \rho_0$. In that case, one might try in practice to tune ν_m in order to make the test react at the desired critical value ρ_c. Generating the (missing) data set at the critical value, from a *modal to data* simulator, might also turn out useful.

A careful evaluation of the sensitivity of the test w.r.t. changes in the critical value ρ_c, and also w.r.t. the choice of θ_0 and of the data sets used for the estimation of the reference $\theta_0, \mathcal{J}, \Sigma$, and extensive tests of the methods on different applications, are the topic of current investigations.

6 Conclusion

Motivated by the flutter monitoring problem, we have described a statistical approach towards fast in-flight on-board detection of flutter onset, combining modal model-based and in-flight data-based methods. The key elements in the design of two statistical detection algorithms for monitoring a damping coefficient have been presented. Both tests handle an output-only subspace-based residual previously proposed by the authors for structural health monitoring [3, 5]. Even though mode-shapes are not monitored, they are explicitly involved in the computation of the proposed tests. It is our experience [4] that this fact may be of crucial importance in structural health monitoring, especially when detecting small deviations in the modal behavior. The first test is covariance-driven and works batch wise. It relies on the asymptotic statistical local approach to monitoring [1]. The second test is temporal data-driven and performs on-line flutter monitoring. It builds on a different asymptotic for the residual, combined with the on-line cumulative sum (CUSUM) test of common use in quality control [2]. On a data set from a *real* flight structure, the latter test has been shown to provide promising results.

References

[1] M. Basseville (1998). On-board component fault detection and isolation using the statistical local approach. *Automatica*, **34**(11), pp.1391-1416.

[2] M. Basseville and I.V. Nikiforov (1993). *Detection of Abrupt Changes - Theory and Application*, Prentice-Hall. `http://www.irisa.fr/sigma2/kniga/`.

[3] M. Basseville, M. Abdelghani and A. Benveniste (2000). Subspace-based fault detection algorithms for vibration monitoring. *Automatica*, **36**(1), pp.101-109.

[4] M. Basseville, L. Mevel and M. Goursat (2003). Statistical model-based damage detection and localization: subspace-based residuals and damage-to-noise sensitivity ratios. *Jal Sound and Vibration*, to appear.

[5] M. Basseville, L. Mevel, A. Vecchio, B. Peeters and H. Van der Auweraer (2003). Output-only subspace-based damage detection – Application to a reticular structure. *Structural Health Monitoring: An International Journal*, Special Issue on the *1st European Workshop on Structural Health Monitoring*, **2**(2), pp.161-168.

[6] M. Basseville, A. Benveniste, M. Goursat, L. Hermans, L. Mevel and H. Van der Auweraer (2001). Output-only subspace-based structural identification: from theory to industrial testing practice. *ASME Journal of Dynamic Systems Measurement and Control*, Special Issue on Identification of Mechanical Systems, **123**(4), pp.668-676.

[7] A. Benveniste, M. Métivier and P. Priouret (1990). *Adaptive Algorithms and Stochastic Approximations*. Springer, New York.

[8] M.J. Brenner, R.C. Lind and D.F. Voracek (1997). Overview of recent flight flutter testing research at NASA Dryden. *NASA Technical Memorandum* **4792**.

[9] M.J. Brenner (2003). Non-stationary dynamics data analysis with wavelet-SVD filtering. *Mechanical Systems and Signal Processing*, **17**(4), pp.765-786.

[10] J.E. Cooper (1995). Parameter estimation methods for flight flutter testing. *80th AGARD Structures and Materials Panels*, CP-566, Rotterdam, NL.

[11] G. Dimitriadis and J.E. Cooper (2001). Flutter prediction from flight flutter test data. *Jal of Aircraft*, **38**(2), pp.355-367.

[12] D.J. Ewins (1984). *Modal Testing: Theory and Practice*. Research Studies Press, Letchworth.

[13] C.R. Farrar, S.W. Doebling and D.A. Nix (2001). Vibration-based structural damage identification. *The Royal Society, Philosophical Transactions: Mathematical, Physical and Engineering Sciences*, **359**(1778), pp.131-150.

[14] E. Feron, M. Brenner, J. Paduano and A. Turevskiy (1998). Time-frequency analysis for transfer function estimation and application to flutter clearance. *Jal of Guidance, Control, and Dynamics*, **21**(3), pp.375-382.

[15] W. Gersch (1974). On the achievable accuracy of structural parameter estimates. *Jal Sound and Vibration*, **34**(1), pp.63-79.

[16] P. Guillaume, P. Verboren and B. Cauberghe (2003). Flight flutter analysis using frequency-domain system identification techniques. *13th IFAC/IFORS Symp. System Identification (SYSID)*, Rotterdam, NL.

[17] M.W. Kehoe (1995). A historical overview of flight flutter testing. *NASA Technical Memorandum* **4720**.

[18] E.L. Lehmann (1986). *Testing Statistical Hypotheses*. Wiley. Series in Probability and Mathematical Statistics, 2nd Ed.

[19] R. Lind (2003a). Flight testing with the flutterometer. *Jal of Aircraft*, **40**(3), pp.574-579.

[20] R. Lind (2003b). Flight test evaluation of flutter prediction methods. *Jal of Aircraft*, **40**(5), pp.964-970.

[21] R. Lind and M. Brenner (1998). Robust flutter margin analysis that incorporates flight data. *NASA Technical Paper* **206543**.

[22] R. Lind and M. Brenner (2000). Flutterometer: an on-line tool to predict robust flutter margins. *Jal of Aircraft*, **37**(6), pp.1105-1112.

[23] L. Mevel, M. Goursat and M. Basseville (2003). Stochastic subspace-based structural identification and damage detection and localization - Application to the Z24 bridge benchmark. *Mechanical Systems and Signal Processing*, **17**(1), pp.143-151.

[24] L. Mevel, M. Goursat and A. Benveniste (2003). Using subspace on flight data, a practical example. *21st International Modal Analysis Conference*, Kissimmee, Fl.

[25] L. Mevel, L. Hermans and H. Van der Auweraer (1999). Application of a subspace-based fault detection method to industrial structures. *Mechanical Systems and Signal Processing*, **13**(6), pp.823-838.

[26] L. Mevel, M. Goursat, M. Basseville and A. Benveniste (2003). Subspace-based modal identification and monitoring of large structures, a Scilab Toolbox. *13th IFAC/IFORS Symp. System Identification (SYSID)*, Rotterdam, NL. `http://www.irisa.fr/sigma2/constructif/modal.htm`

[27] B. Peeters and G. De Roeck (1999). Reference-based stochastic subspace identification for output-only modal analysis. *Mechanical Systems and Signal Processing*, **13**(6), pp.855-878.

[28] C.R. Pickrel and P.J. White (2003). Flight flutter testing of transport aircraft: in-flight modal analysis. *21st International Modal Analysis Conference*, Kissimmee, Fl.

[29] S. Prudhomme, C. Blondeau, M. Hubert and A. Bucharles (1999). An unsteady aerodynamics identification procedure for flutter prediction. *International Forum on Aeroelasticity*, Williamsburg, VA. *ONERA Report* **TP 101**.

[30] P. Stoïca and R.L. Moses (1997). *Introduction to Spectral Analysis*, Prentice Hall.

[31] A. Turevskiy, E. Feron and J. Paduano (1999). Flutter boundary prediction using physical models and experimental data. *Jal of Guidance, Control, and Dynamics*, **22**(1), pp.168-171.

[32] P. Van Overschee and B. De Moor (1996). *Subspace Identification for Linear Systems: Theory – Implementation – Methods*. Kluwer.

[33] P. Verboven, B. Cauberghe, P. Guillaume, S. Vanlanduit and E. Parloo (2003). Modal parameter estimation and monitoring for on-line flight flutter analysis. *Mechanical Systems and Signal Processing*, to appear.

[34] M. Viberg, B. Wahlberg and B. Ottersten (1997). Analysis of state space system identification methods based on instrumental variables and subspace fitting. *Automatica*, **33**(9), pp.1603-1616.

[35] Q. Zhang and M. Basseville (2003). Advanced numerical computation of χ^2-tests for fault detection and isolation. *5th IFAC/IMACS Symp. SAFEPROCESS*, Washington D.C., USA.

[36] Q. Zhang, M. Basseville and A. Benveniste (1994). Early warning of slight changes in systems and plants with application to condition based maintenance. *Automatica*, **30**(1), pp.95-114.

[37] N.H. Zimmerman and J.T. Weissenburger (1964). Prediction of flutter onset speed based on flight testing at subcritical speeds. *Jal of Aircraft*, **1**(4), pp.190-202.

Contents

1 Introduction **3**

2 Subspace-based modal identification and monitoring **5**
2.1 Modeling and parameterizations 5
2.2 Residual associated with subspace identification 7
2.3 On-board χ^2-test for modal monitoring 9
2.4 Modal diagnosis 10

3 Flutter monitoring - First test, working batch wise **11**
3.1 A one-sided test 11

4 Flutter monitoring - Second test, working on-line **12**
4.1 Another insight in the residual 13
4.2 The CUSUM test 13
4.3 The proposed on-line flutter test 14

5 Experimental analysis **16**
5.1 Implementation and tuning issues 16
5.2 Experimental results 17
5.3 Discussion 17

6 Conclusion **19**

References **20**

Unité de recherche INRIA Lorraine, Technopôle de Nancy-Brabois, Campus scientifique,
615 rue du Jardin Botanique, BP 101, 54600 VILLERS LÈS NANCY
Unité de recherche INRIA Rennes, Irisa, Campus universitaire de Beaulieu, 35042 RENNES Cedex
Unité de recherche INRIA Rhône-Alpes, 655, avenue de l'Europe, 38330 MONTBONNOT ST MARTIN
Unité de recherche INRIA Rocquencourt, Domaine de Voluceau, Rocquencourt, BP 105, 78153 LE CHESNAY Cedex
Unité de recherche INRIA Sophia-Antipolis, 2004 route des Lucioles, BP 93, 06902 SOPHIA-ANTIPOLIS Cedex

Éditeur
INRIA, Domaine de Voluceau, Rocquencourt, BP 105, 78153 LE CHESNAY Cedex (France)
http://www.inria.fr
ISSN 0249-6399